An equilibrium-based stress recovery procedure for the VEM

An equilibrium-based stress recovery procedure for the VEM

E. Artioli[a], S. de Miranda[b], C. Lovadina[c,d], L. Patruno [b,e*]

[a] *Department of Civil Engineering and Computer Science, University of Rome Tor Vergata, Via del Politecnico 1, 00133 Rome, Italy*

[b] *DICAM, University of Bologna, Viale Risorgimento 2, 40136 Bologna, Italy*

[c] *Dipartimento di Matematica, Università degli Studi di Milano, Via Saldini 50, 20133 Milano, Italy*

[d] *IMATI del CNR, Via Ferrata 1, 27100 Pavia, Italy*

[e] *WERC, Tamkang University, Yingzhuan Road, Tamsui District, New Taipei City, Taiwan*

Abstract

Within the framework of the displacement-based Virtual Element Method (VEM), namely for plane elasticity, an important topic is the development of optimal techniques for the evaluation of the stress field. In fact, in the classical VEM formulation, the same projection operator used to approximate the strain field (and then evaluate the stiffness matrix) is employed to recover, via constitutive law, the stress field. Considering a first-order formulation, strains are locally mapped onto constant functions, and stresses are piecewise constant. However, the virtual displacements might engender more complex strain fields for polygons which are not triangles. This leads to an undesirable loss of information with respect to the underlying virtual stress field. The Recovery by Compatibility in Patches, originally proposed for Finite Element schemes, is here extended to VEM aiming at mitigating such an effect. Stresses are recovered by minimizing the complementary energy of patches of elements over an assumed set of equilibrated stress modes. The procedure is simple, efficient and can be readily implemented in existing codes. Numerical tests confirm the good performance of the proposed technique in terms of accuracy and indicate an increase of convergence rate with respect to the classical approach in many cases.

Keywords: Virtual Element Method, Stress recovery, RCP

*Corresponding author

Email address: luca.patruno@unibo.it (L. Patruno [b,e])

1. Introduction

The Virtual Element Method (VEM) is a relatively new and very powerful discretisation scheme which is rapidly attracting the interest of the scientific community. The technique is well-known for its formal elegance and flexibility, which allows using meshes composed of general polygons/polyhedra, and allowing for the presence of hanging nodes and nonconforming grids [1, 2, 3, 4]. The method, originally proposed in 2012 in its displacement-based formulation and presented for the Laplace operator in a two-dimensional context [1], is rapidly developing and has been already applied to numerous physical problems [3, 5, 6, 7, 8, 9, 10, 11, 12, 13, 14, 15] as well as extended to three-dimensional cases [16] and mixed formulations [17, 18, 19].

Differently from the Finite Element (FE) framework, in the virtual element technique the local polynomial approximation concept is abandoned and the functions used for the discretisation procedure are not known pointwise, in general. However, a careful selection of the degrees of freedom and the assumption that the unknown fields satisfy appropriate differential equations, make it possible to compute the stiffness matrix and the load vector. In particular, for plane elasticity problems, classical VEM formulations assume that displacements are completely known only at the element boundaries while the internal field, for high-order schemes, is characterised only by means of internal degrees of freedom representing appropriate integral quantities.

Due to the virtual nature of the displacement field, strains (the symmetric gradient of the displacements) are not directly computable and need to be further approximated in order to compute the stiffness matrix. The standard procedure consists in defining a strain field, polynomial inside the element, which can be determined from the displacement degrees of freedom. For example, in the case of the first-order formulation, the aforementioned strategy leads to constant strains inside the elements, irrespective of the number of element edges, and thus irrespective of the number of displacement degrees of freedom. Therefore, applying the constitutive law, the recovered stress field is essentially piecewise constant as well. As it can be easily realised, this leads to an undesirable loss of information with respect to the underlying virtual stress field, especially for meshes consisting of polygons with numerous edges, and often leads to results that are not completely satisfactory.

In the context of FE discretization schemes, stress recovery techniques received considerable attention in the last decades [20]. In particular, the Superconvergent Patch Recovery (SPR) procedure proposed by Zienkiewicz and Zhu [21, 22] clearly highlighted the remarkable advantages which might be obtained by appropriately postprocessing the stress field provided by the FE formulation. In particular, in the original SPR procedure, the recovery is performed by calculating stresses as a least-square interpolation of values evaluated at superconvergent points. Later, the procedure has been refined [23, 24, 25, 26, 27, 28] introducing, for example, equilibrium constraints in order to lead to more accurate results.

Another well-known technique is the Recovery by Equilibrium in Patches

(REP) proposed in [29, 30, 31]. The idea behind the REP is to impose the fulfillment of equilibrium on the patch in a weak form while proceeding to a reinterpolation of stresses on a local polynomial base. Combinations of elementwise and boundary equilibrium conditions to be added to the standard REP formulation have been also proposed in order to enhance the accuracy of the obtained results [29]. Other interesting examples of recovery procedures based on equilibrium considerations have been proposed, for instance, in [32, 33, 34] and, more recently, in [35] where the devised technique is adopted in order to calculate error bounds for the advection-diffusion-reaction equation.

In this context, the Recovery by Compatibility in Patches (RCP), originally proposed in [36] for FE schemes, has shown to have very good properties in terms of simplicity and robustness. Moreover, it has been already successfully applied to *a posteriori* error estimation [37] as well as to drive adaptive mesh refinement [38]. Moreover, it has been shown to be particularly well suited for transverse stresses profile reconstruction in plate bending problems for which, thanks to its equilibrating nature, it leads to the automatic fulfillment of the pointwise equilibrium at the plate top and bottom surfaces [39].

The key idea underlying RCP is to minimise the complementary energy associated to a patch of elements treated as an isolated system among a set of equilibrated stress fields. In particular, on each patch, stresses are approximated as a linear combination of self-equilibrated stress modes enriched by an appropriate particular solution. It is worth to note that the explicit knowledge of the displacements is required only along the patch boundaries, so rendering the RCP approach naturally well-suited for virtual element schemes.

With this in mind, the RCP is here extended to VEM in order to mitigate the loss of information induced by the aforementioned projection operator, normally employed in order to calculate the stress/strain fields, so allowing to take full advantage of the VEM formulation. In particular, the proposed technique is here tested considering two variants: in the first one, a degenerate patch composed of a single polygon is considered. For triangles, this does not significantly improve the results obtained using the classical strain computation. However, the benefit becomes apparent when the number of edges increases. In the second one, RCP is presented by considering patches of elements in analogy to its original formulation, developed in the context of finite elements schemes.

The paper is organised as follows. In Section 2, the VEM formulation for plane elasticity problems is briefly recalled. Then, the RCP procedure is introduced in Section 3. Numerical results are presented for a wide selection of test cases in Section 4 and, finally, conclusions are drawn in Section 5.

2. Virtual Element Method

Consider a body occupying a region Ω of the two-dimensional space on which a reference system (O, x, y) is introduced. Let us denote with the symbol $\partial\Omega$ the boundary of such a body and consider the case of homogeneous Dirichlet boundary conditions. Other types of boundary conditions can be treated in

the same spirit of finite element schemes. Denoting as $\mathbf{u}(x,y) = [u,v]^T$, the displacement field, the associated strains are defined as

$$\boldsymbol{\varepsilon}(\mathbf{u}) = \mathbf{D}\mathbf{u} \qquad \text{with} \qquad \mathbf{D} = \begin{bmatrix} \partial_x & 0 \\ 0 & \partial_y \\ \partial_y & \partial_x \end{bmatrix}, \tag{2.1}$$

where $\mathbf{D}$ represents the differential compatibility operator. The plane elasticity problem can be thus expressed as: find $\mathbf{u} \in \mathbf{v}$ such that

$$\int_\Omega \boldsymbol{\varepsilon}(\mathbf{v})^T \boldsymbol{C}\boldsymbol{\varepsilon}(\mathbf{u}) = \int_\Omega \mathbf{v}^T \boldsymbol{b} \qquad \forall \mathbf{v} \in \mathbf{v}, \tag{2.2}$$

where $\boldsymbol{C}$ is the elastic matrix, $\mathbf{v}$ is the space of the kinematically admissible displacements, $\boldsymbol{b}$ is the applied external load.

In order to build a VEM scheme, it is assumed that Ω is subdivided into non-overlapping polygons with straight edges. In the following, E indicates one and each of such polygons, ∂E denotes its boundary while e denotes one and each of the edges of E. Moreover, we here assume a homogeneous material, but inhomogeneous bodies can be treated as well (cf. for instance [18, 40]) We introduce a local approximation space, $\mathbf{v}_{h|E}$, whose elements are typically not known pointwise, but are determined by means of a suitable set of degrees of freedom (thus, $\mathbf{v}_{h|E}$ is said to be *virtual*).

In the following, reference is made to a first-order VEM discretisation scheme. The space $\mathbf{v}_{h|E}$ is chosen so that

$$\mathbf{v}_{h|E} = \left\{ \mathbf{v}_h \in H^1(E) \cap C^0(E) : \mathbf{D}^\star(\boldsymbol{C}\boldsymbol{\varepsilon}(\mathbf{v}_h)) = \mathbf{0},\ \mathbf{v}_{h|e} \in \boldsymbol{P}_1(e) \quad \forall e \in \partial E \right\}, \tag{2.3}$$

where $\mathbf{D}^\star$ is the formal adjoint of $\mathbf{D}$ while $\boldsymbol{P}_1(e)$ indicates the space of linear functions on the edges of E.

A set of degrees of freedom which can be used in order to describe such a space is represented by the values of the displacements at the element vertices. It must be noticed that, thanks to the requirements expressed in Eq. (2.3), displacements must be linear on edges so that the vertex values completely characterise the displacement field on ∂E. A sketch of the virtual field and of the considered degrees of freedom is provided in Fig. 1.

Due to the virtual nature of the approximating functions, it is not possible to directly compute the terms of Eq. (2.2), and especially the left-hand side. It is thus necessary to introduce an operator, $\boldsymbol{\Pi} : \mathbf{v}_{h|E} \to \boldsymbol{P_0}(E)$, defined as

$$\int_E \boldsymbol{\Pi}(\mathbf{v}_h)^T \boldsymbol{\varepsilon}^0 = \int_E \boldsymbol{\varepsilon}(\mathbf{v}_h)^T \boldsymbol{\varepsilon}^0 \qquad \forall \boldsymbol{\varepsilon}^0 \in \boldsymbol{P}_0(E). \tag{2.4}$$

Above, $\boldsymbol{P}_0(E)$ denotes the space of constant fields over the element. It can be observed that $\boldsymbol{\Pi}$ is an operator which maps the virtual displacements onto constant strain fields. A typical displacement and strain field can be formally represented as

$$\mathbf{v}_h = \boldsymbol{N}^V \tilde{\mathbf{v}}_h, \qquad \boldsymbol{\varepsilon}^0 = \boldsymbol{N}^P \tilde{\boldsymbol{\varepsilon}}, \tag{2.5}$$

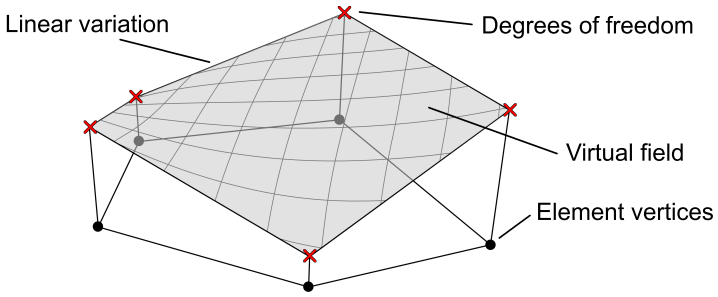

Figure 1: Sketch of the virtual function and of the considered degrees of freedom.

where the vector $\tilde{\mathbf{v}}_h$ collects the degrees of freedom (i.e. the values of the displacements at the polygon vertices) while $\tilde{\boldsymbol{\varepsilon}}$ is a vector collecting the degrees of freedom of the approximated strain field. The term $\boldsymbol{N}^V$ collects virtual displacement shape functions and, thus, is not explicitly known, while $\boldsymbol{N}^P$, still considering a first order scheme, takes the form

$$\boldsymbol{N}^P = \begin{bmatrix} 1 & 0 & 0 \\ 0 & 1 & 0 \\ 0 & 0 & 1 \end{bmatrix}. \tag{2.6}$$

Indicating as $\boldsymbol{\Pi}^m$ the $\boldsymbol{\Pi}$ operator expressed as a matrix, it is possible to write the discrete strains as

$$\boldsymbol{\Pi}(\mathbf{v}_h) = \boldsymbol{N}^P \boldsymbol{\Pi}^m \tilde{\mathbf{v}}_h. \tag{2.7}$$

The operator $\boldsymbol{\Pi}^m$ can be thus evaluated by means of Eq. (2.4). In particular, substituting Eq. (2.7) into Eq. (2.4), we obtain

$$\int_E (\boldsymbol{N}^P \boldsymbol{\Pi}^m \tilde{\mathbf{v}}_h)^T \boldsymbol{N}^P \tilde{\boldsymbol{\varepsilon}} = \int_E \left[\boldsymbol{\varepsilon}(\boldsymbol{N}^V \tilde{\mathbf{v}}_h)\right]^T \boldsymbol{N}^P \tilde{\boldsymbol{\varepsilon}} \qquad \forall \tilde{\boldsymbol{\varepsilon}} \in \mathbb{R}^3, \tag{2.8}$$

which, integrated by parts, leads to

$$\int_E (\boldsymbol{N}^P \boldsymbol{\Pi}^m \tilde{\mathbf{v}}_h)^T \boldsymbol{N}^P \tilde{\boldsymbol{\varepsilon}} = \int_{\partial E} (\boldsymbol{N}^V \tilde{\mathbf{v}}_h)^T \boldsymbol{\mathcal{N}}_E \boldsymbol{N}^P \tilde{\boldsymbol{\varepsilon}} \qquad \forall \tilde{\boldsymbol{\varepsilon}} \in \mathbb{R}^3, \tag{2.9}$$

where, denoting the outward normal as $\boldsymbol{n} = [n_x, n_y]^T$, $\boldsymbol{\mathcal{N}}_E$ is

$$\boldsymbol{\mathcal{N}}_E = \begin{bmatrix} n_x & 0 & n_y \\ 0 & n_y & n_x \end{bmatrix}. \tag{2.10}$$

Equation (2.9) can be rewritten as

$$\tilde{\boldsymbol{\varepsilon}}^T \mathcal{G} \boldsymbol{\Pi}^m \tilde{\mathbf{v}}_h = \tilde{\boldsymbol{\varepsilon}}^T \mathcal{B} \tilde{\mathbf{v}}_h \qquad \forall \tilde{\boldsymbol{\varepsilon}} \in \mathbb{R}^3, \tag{2.11}$$

where

$$\mathcal{G} = \int_E (\boldsymbol{N}^P)^T \boldsymbol{N}^P, \qquad \mathcal{B} = \int_{\partial E} (\boldsymbol{\mathcal{N}}_E \boldsymbol{N}^P)^T \boldsymbol{N}^V. \tag{2.12}$$

Equation (2.11) allows to compute $\mathbf{\Pi}^m$ as the solution of a linear system while matrices $\mathcal{G}$ and $\mathcal{B}$ are computable because displacements appear only at the boundary where they are explicitly known. This leads to the evaluation of $\mathbf{\Pi}^m$ as

$$\mathbf{\Pi}^m = \mathcal{G}^{-1}\mathcal{B}, \tag{2.13}$$

and, thus, to approximate the l.h.s. of Eq. (2.2) as

$$\int_\Omega \boldsymbol{\varepsilon}(\mathbf{v})^T \boldsymbol{C}\boldsymbol{\varepsilon}(\mathbf{u}) \approx \int_\Omega (\mathbf{\Pi}^m \tilde{\mathbf{v}_h})^T \boldsymbol{C}\mathbf{\Pi}^m \tilde{\mathbf{u}_h}. \tag{2.14}$$

After algebraic manipulations, it is possible to identify the stiffness matrix, $\boldsymbol{K}_c$, as

$$\boldsymbol{K}_c = \mathcal{B}^T\mathcal{G}^{-T}\left[\int_E (\boldsymbol{N}^P)^T \boldsymbol{C}\boldsymbol{N}^P\right]\mathcal{G}^{-1}\mathcal{B}. \tag{2.15}$$

In order to ensure that $\boldsymbol{K}_c$ has the correct rank, a stabilisation term $\boldsymbol{K}_s$ (not further discussed here) must be added to $\boldsymbol{K}_c$ so that the stiffness matrix is usually redefined as $\boldsymbol{K} = \boldsymbol{K}_c + \boldsymbol{K}_s$. For further details, we refer to [2, 7], for example.

It is important to notice that the operator $\mathbf{\Pi}^m$ leads to constant strain fields while the virtual displacements are assumed to be linear over the element edges, and lead to divergence-free stress distributions (cf. Eq. (2.3) and Fig. 1).

For a triangular element, the virtual (low-order) formulation is equivalent to the standard (low-order) triangular finite element. However, when polygons with a higher number of edges are considered, the degrees of freedom used to describe the displacement field could, in principle, give rise to stress/strain fields richer than the constant ones. A kind of loss of information is thus expected when using operator $\mathbf{\Pi}^m$ to compute the stresses.

In the following, RCP is introduced as a postprocessing technique for the VEM procedure, with the aim of improving the accuracy of the obtained stresses.

3. Recovery by Compatibility in Patches

The key idea of RCP is to minimise the complementary energy associated to a patch of elements treated as an isolated system among a set of equilibrated stress modes [36]. In the following, RCP is presented for degenerate patches composed of a single virtual element. The generalisation of the procedure to the case of patches composed of more than one element does not introduce substantial modifications and is presented in Section 3.2.

To begin, we recall that the elasticity problem may be written in mixed variables as:

$$\begin{cases} \text{Find } (\boldsymbol{\sigma}, \mathbf{u}) \text{ such that} \\ \mathbf{D}^\star\boldsymbol{\sigma} = \mathbf{b} \qquad \text{in } \Omega \\ \boldsymbol{\sigma} = \boldsymbol{C}\boldsymbol{\varepsilon}(\mathbf{u}) \qquad \text{in } \Omega \\ + \text{ boundary conditions} \end{cases} \tag{3.1}$$

We notice that, if $(\boldsymbol{\sigma}, \mathbf{u})$ is the solution to problem (3.1), then for every element E, $\boldsymbol{\sigma}$ minimizes the complementary energy

$$J^c(\boldsymbol{\tau}) = \frac{1}{2}\int_E \boldsymbol{\tau}^T \boldsymbol{C}^{-1}\boldsymbol{\tau} - \int_{\partial E} \mathbf{u}^T \boldsymbol{\mathcal{N}}_E \boldsymbol{\tau} \tag{3.2}$$

over the affine space $\boldsymbol{\Sigma}_{\mathbf{b}}(E)$, defined by

$$\boldsymbol{\Sigma}_{\mathbf{b}}(E) := \{\boldsymbol{\tau} \in H(\mathbf{D}^\star; E) \ : \ \mathbf{D}^\star\boldsymbol{\tau} + \mathbf{b} = \mathbf{0}\}. \tag{3.3}$$

Above, $H(\mathbf{D}^\star; E)$ is the space of symmetric tensor fields, whose components are in $L^2(E)$, and for which $\mathbf{D}^\star\boldsymbol{\tau}$ is in $L^2(E)^2$ as well. We remark that such a space is typically denoted as $H(\mathbf{div}, E)$ in the mathematical literature (see [41], for instance).

Supposing that the analytical solution $\mathbf{u}$ *is given on the boundary* ∂E, the stress field $\boldsymbol{\sigma}$ is then the solution of the variational problem:

$$\begin{cases} \text{Find } \boldsymbol{\sigma} \in \boldsymbol{\Sigma}_{\mathbf{b}}(E) \text{ such that} \\ \displaystyle\int_E \boldsymbol{\tau}_{\mathbf{0}}^T \boldsymbol{C}^{-1}\boldsymbol{\sigma} - \int_{\partial E} \mathbf{u}^T \boldsymbol{\mathcal{N}}_E \boldsymbol{\tau}_{\mathbf{0}} = 0 \qquad \forall \boldsymbol{\tau}_{\mathbf{0}} \in \boldsymbol{\Sigma}_{\mathbf{0}}(E). \end{cases} \tag{3.4}$$

Above, $\boldsymbol{\Sigma}_{\mathbf{0}}(E)$ is defined by Eq. (3.3), choosing $\mathbf{b} = \mathbf{0}$. Given a *fixed* particular stress field $\boldsymbol{\sigma}_{\mathbf{b}} \in \boldsymbol{\Sigma}_{\mathbf{b}}(E)$, the splitting

$$\boldsymbol{\sigma} = \boldsymbol{\sigma}_{\mathbf{0}} + \boldsymbol{\sigma}_{\mathbf{b}}, \text{ with } \boldsymbol{\sigma}_{\mathbf{0}} \in \boldsymbol{\Sigma}_{\mathbf{0}}(E), \tag{3.5}$$

shows that problem (3.4) is equivalent to:

$$\begin{cases} \text{Find } \boldsymbol{\sigma}_{\mathbf{0}} \in \boldsymbol{\Sigma}_{\mathbf{0}}(E) \text{ such that} \\ \displaystyle\int_E \boldsymbol{\tau}_{\mathbf{0}}^T \boldsymbol{C}^{-1}\boldsymbol{\sigma}_{\mathbf{0}} = \int_{\partial E} \mathbf{u}^T \boldsymbol{\mathcal{N}}_E \boldsymbol{\tau}_{\mathbf{0}} - \int_E \boldsymbol{\tau}_{\mathbf{0}}^T \boldsymbol{C}^{-1}\boldsymbol{\sigma}_{\mathbf{b}} \qquad \forall \boldsymbol{\tau}_{\mathbf{0}} \in \boldsymbol{\Sigma}_{\mathbf{0}}(E). \end{cases} \tag{3.6}$$

We remark that: (1) the bilinear form $(\boldsymbol{\sigma}_{\mathbf{0}}, \boldsymbol{\tau}_{\mathbf{0}}) \to \int_E \boldsymbol{\tau}_{\mathbf{0}}^T \boldsymbol{C}^{-1}\boldsymbol{\sigma}_{\mathbf{0}}$ is continuous and coercive over $\boldsymbol{\Sigma}_{\mathbf{0}}(E)$; (2) given $\mathbf{u}$ and $\boldsymbol{\sigma}_{\mathbf{b}}$, the right-hand side is a linear and continuous functional on $\boldsymbol{\Sigma}_{\mathbf{0}}(E)$. Therefore, problem (3.6) is stable. It must be noticed that such subdivision of the stress field in a homogeneous and a particular solution corresponds to a well-established technique, often adopted in order to build stress approximations in the context of equilibrium and hybrid stress finite elements [42, 43]. With this in mind, the idea of the RCP procedure is to recover the stress field for every element E, by solving problem (3.6) where the displacement on the boundary ∂E comes from the VEM solution, i.e. $\mathbf{u}_h$.

Therefore, it is natural to consider the following *continuous problem with approximated displacements*:

$$\begin{cases} \text{Find } \widetilde{\boldsymbol{\sigma}}_{\mathbf{0}} \in \boldsymbol{\Sigma}_{\mathbf{0}}(E) \text{ such that} \\ \displaystyle\int_E \boldsymbol{\tau}_{\mathbf{0}}^T \boldsymbol{C}^{-1}\widetilde{\boldsymbol{\sigma}}_{\mathbf{0}} = \int_{\partial E} \mathbf{u}_h^T \boldsymbol{\mathcal{N}}_E \boldsymbol{\tau}_{\mathbf{0}} - \int_E \boldsymbol{\tau}_{\mathbf{0}}^T \boldsymbol{C}^{-1}\boldsymbol{\sigma}_{\mathbf{b}} \qquad \forall \boldsymbol{\tau}_{\mathbf{0}} \in \boldsymbol{\Sigma}_{\mathbf{0}}(E). \end{cases} \tag{3.7}$$

We point out that, in general, the analytical solution of the local problem (3.7) $\widetilde{\boldsymbol{\sigma}}_{\mathbf{0}}$ is not equal to $\boldsymbol{\sigma}_{\mathbf{0}}$ (cf. (3.6)). As a consequence, the corresponding stress field $\widetilde{\boldsymbol{\sigma}} = \widetilde{\boldsymbol{\sigma}}_{\mathbf{0}} + \boldsymbol{\sigma}_{\mathbf{b}}$ is different from the actual stress field $\boldsymbol{\sigma} = \boldsymbol{\sigma}_{\mathbf{0}} + \boldsymbol{\sigma}_{\mathbf{b}}$ (see (3.5)).

The RCP procedure may be interpreted as an approximation of problem (3.7). More precisely, one chooses a suitable polynomial space $\boldsymbol{\Sigma}_{\mathbf{0},h}(E) \subset \boldsymbol{\Sigma}_{\mathbf{0}}(E)$ and solve:

$$\begin{cases} \text{Find } \widetilde{\boldsymbol{\sigma}}_{0,h} \in \boldsymbol{\Sigma}_{\mathbf{0},h}(E) \text{ such that} \\ \displaystyle\int_E \boldsymbol{\tau}_{\mathbf{0},h}^T \boldsymbol{C}^{-1} \widetilde{\boldsymbol{\sigma}}_{\mathbf{0},h} = \int_{\partial E} \mathbf{u}_h^T \boldsymbol{\mathcal{N}}_E \boldsymbol{\tau}_{\mathbf{0},h} - \int_E \boldsymbol{\tau}_{\mathbf{0},h}^T \boldsymbol{C}^{-1} \boldsymbol{\sigma}_{\mathbf{b}} \qquad \forall \boldsymbol{\tau}_{\mathbf{0},h} \in \boldsymbol{\Sigma}_{\mathbf{0},h}(E). \end{cases} \tag{3.8}$$

The recovered stress field on the element E is then defined by

$$\widetilde{\boldsymbol{\sigma}}_h = \widetilde{\boldsymbol{\sigma}}_{\mathbf{0},h} + \boldsymbol{\sigma}_{\mathbf{b}}. \tag{3.9}$$

3.1. RCP implementation

The homogeneous part $\widetilde{\boldsymbol{\sigma}}_{\mathbf{0}}$ is approximated as

$$\widetilde{\boldsymbol{\sigma}}_{\mathbf{0},h} = \boldsymbol{P}\boldsymbol{\beta}, \tag{3.10}$$

where $\boldsymbol{P}$ is a matrix of preselected self-equilibrated stress modes, while $\boldsymbol{\beta}$ is the vector of the unknown parameters. Then, if a linear approximation is adopted for $\widetilde{\boldsymbol{\sigma}}_{\mathbf{0},h}$, $\boldsymbol{P}$ takes the form

$$\boldsymbol{P} = \begin{bmatrix} 1 & 0 & 0 & y & 0 & x & 0 \\ 0 & 1 & 0 & 0 & x & 0 & y \\ 0 & 0 & 1 & 0 & 0 & -y & -x \end{bmatrix}. \tag{3.11}$$

The particular solutions, $\boldsymbol{\sigma}_{\mathbf{b}}$, appearing in Eq. (3.5) can be calculated as

$$\boldsymbol{\sigma}_{\mathbf{b}} = \begin{bmatrix} \sigma_x \\ \sigma_y \\ \tau_{xy} \end{bmatrix}_{\mathbf{b}} = \begin{bmatrix} -I_x(b_x) \\ -I_y(b_y) \\ 0 \end{bmatrix}. \tag{3.12}$$

Above, b_x and b_y are the body force components. Furthermore, $I_x(b_x)$ is an antiderivative of b_x with respect to the coordinate x, i.e. it holds $\frac{\partial}{\partial x} I_x(b_x) = b_x$. Analogous definition applies to $I_y(b_y)$ with respect to the coordinate y. Indeed, although the choice of the particular solution is arbitrary, being the only requirement the equilibrium with the applied body forces, its combination with the homogeneous solution is univocally determined up to terms of degree equal to the degree of completeness of the homogeneous solution. If the antiderivatives for b_x or b_y are not explicitly known, we first approximate the body force within the element by a constant field, then we take the corresponding antiderivatives. Such an approach corresponds to a linear approximation of the particular solution within each element. Higher order approximations might

be easily developed considering polynomial approximations of the applied body forces.

Substituting Eq. (3.10) into Eq. (3.2) leads to

$$J^c(\boldsymbol{\beta}) = \frac{1}{2}\int_E (\boldsymbol{P}\boldsymbol{\beta}+\boldsymbol{\sigma}_{\mathbf{b}})^T \boldsymbol{C}^{-1}(\boldsymbol{P}\boldsymbol{\beta}+\boldsymbol{\sigma}_{\mathbf{b}}) - \int_{\partial E} \mathbf{u}_h^T \boldsymbol{\mathcal{N}}_E(\boldsymbol{P}\boldsymbol{\beta}+\boldsymbol{\sigma}_{\mathbf{b}}). \quad (3.13)$$

Imposing null variations of the functional expressed in Eq. (3.14), the following is obtained

$$\boldsymbol{H}\boldsymbol{\beta} = \boldsymbol{g}, \quad (3.14)$$

where

$$\boldsymbol{H} = \int_E \boldsymbol{P}^T\boldsymbol{C}^{-1}\boldsymbol{P}, \qquad \boldsymbol{g} = \int_{\partial E} \boldsymbol{P}^T\boldsymbol{\mathcal{N}}_E^T\mathbf{u}_h - \int_E \boldsymbol{P}^T\boldsymbol{C}^{-1}\boldsymbol{\sigma}_{\mathbf{b}}. \quad (3.15)$$

In the definition of $\boldsymbol{g}$, see Eq. (3.15), the first term can be integrated by parts and, exploiting that the stress modes are divergence-free, we get

$$\int_{\partial E} \boldsymbol{P}^T\boldsymbol{\mathcal{N}}_E^T\mathbf{u}_h = \int_E \boldsymbol{P}^T\boldsymbol{\varepsilon}(\mathbf{u}_h). \quad (3.16)$$

In the finite element framework, the vector $\boldsymbol{g}$ can be computed using the left-hand side or the right-hand side of Eq. (3.16), leading to identical results. On the contrary, when virtual element schemes are considered, the left-hand side should be used, since the displacements are pointwise known only at the element boundary.

3.2. Patch-based version

The adoption of a patch of elements instead of a single element does not introduce significant additional complexity. For each element E, we consider a given patch $\pi(E)$ of surrounding elements (E is included in $\pi(E)$, i.e. $E \subseteq \pi(E)$). Then, the integrals appearing in Eq. (3.15) are computed over the entire patch $\pi(E)$. Notice that, in this case, the boundary appearing in Eq. (3.15) becomes the boundary $\partial\pi(E)$ of the patch $\pi(E)$. The recovered stress solution on the element E is simply the restriction to E of the computed stress on $\pi(E)$.

Figure 2 provides examples of the patches adopted in the following numerical tests. In particular, *Patch 0* indicates the degenerate case of a single element, *Patch 1* is a patch obtained by considering all surrounding elements sharing at least one node with a central element, while *Patch 1B* represents a *boundary* patch of the same type as *Patch 1*.

As a last remark it is worth noticing that the proposed approach can be easily extended to high-order schemes. In particular, the polynomial representation of the homogeneous part of the stress field $\boldsymbol{P}$ can be enriched in order to become a complete representation base of equilibrated stress fields up to an arbitrary degree (see for instance [39]). Numerous variants of the presented techniques can be developed by varying the underlying VEM formulation, $\boldsymbol{P}$, the size of the patch (i.e. the number of hems around the central element used to identify the

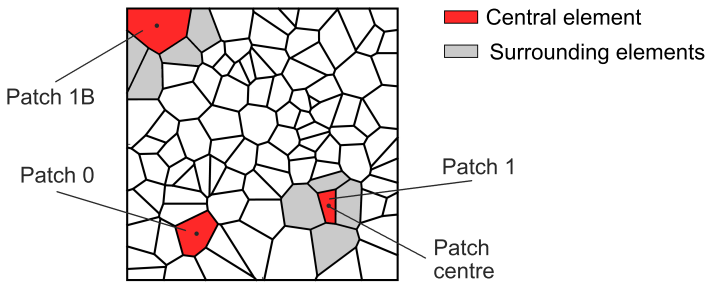

Figure 2: Patch types used in the present study.

patch) and their construction procedure (e.g. node patches might be considered [37]).

Additionally, although the procedure has been developed and presented for two-dimensional elasticity problems, thanks to its simple and clear variational background, it can be easily adopted to three-dimensional cases as well as inelastic problems [44].

4. Numerical results

In this section, numerical tests are used in order to validate the proposed stress recovery procedure. In particular, a square domain characterised by edge length equal to unity is considered. The body is assumed to be homogeneous and isotropic and its mechanical parameters are assigned in terms of the Lamé constants $\lambda = 1$ and $\mu = 1$ [45, 7]. Plane strain regime is assumed.

Indicating as $\boldsymbol{\sigma}^{ex}$ the analytical stress field, the following error norm is used in order to evaluate the accuracy of the obtained results

$$E_\sigma = \left(\int_\Omega (\boldsymbol{\sigma}^{ex} - \widetilde{\boldsymbol{\sigma}}_h)^T \boldsymbol{C}^{-1} (\boldsymbol{\sigma}^{ex} - \widetilde{\boldsymbol{\sigma}}_h) \right)^{1/2} . \tag{4.1}$$

In the subsequent developments such error norm is often normalized with respect to the square root of the strain energy of the exact solution. Furthermore, when the logarithm of such quantities are considered, it should be always intended that base ten is adopted.

As it can be seen in Fig. 3, eight meshes are considered. Four of them are structured and are indicated with the letter 'S' in the following. Those are composed of triangles, quadrilaterals, hexagons and a mixture of convex and concave quadrangles. The remaining four are unstructured meshes composed of triangles, quadrilaterals, random polygons and concave hexagons. Those meshes are indicated with the letter 'U'. The average edge length is indicated as $\bar{h}_e$.

Prescribed displacements are assumed and the corresponding body forces are calculated. Such body forces are then applied to the body, together with Dirichlet conditions over the entire boundary. Three tests are considered:

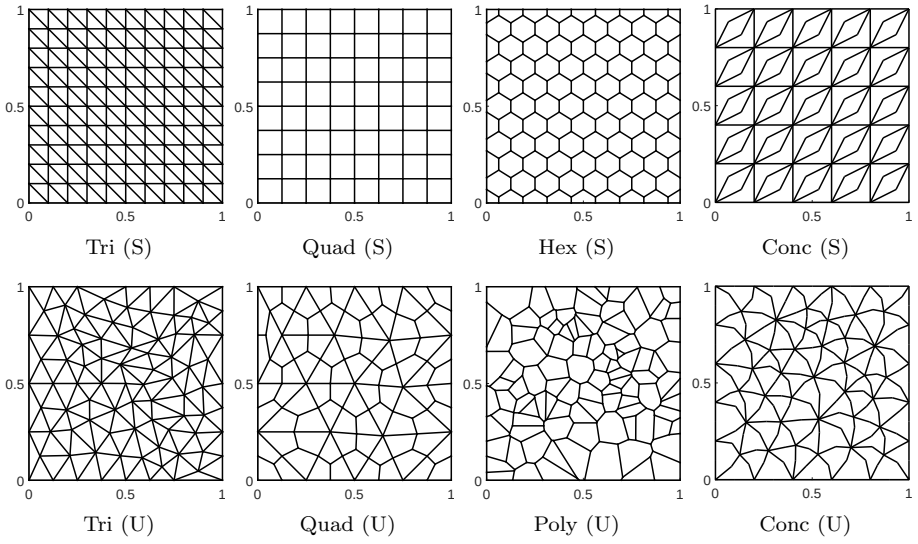

Figure 3: Overview of adopted meshes for convergence assessment numerical tests [18].

- **Test a**: $u_x = x^3 - 3xy^2,\ u_y = y^3 - 3x^2y$;
- **Test b**: $u_x = u_y = \sin(\pi x)\sin(\pi y)$;
- **Test c**: $u_x = xy\sin(\pi x)\sin(\pi y),\ u_y = 0$.

In particular, *Test a* is characterised by polynomial solution and engenders null body forces with inhomogeneous Dirichlet boundary conditions, while in *Test b* the displacement solution is trigonometric and is characterised by homogeneous Dirichlet boundary conditions, see [18]. Analogously to *Test b*, *Test c* is characterised by homogeneous Dirichlet boundary conditions, and u_x is a product of polynomial and trigonometric functions, while u_y vanishes.

Three stress recovery procedures are compared and denoted as *VEM*, *RCP0* and *RCP1*. In particular, *VEM* corresponds to the standard procedure based on the adoption of the operator $\mathbf{\Pi}^m$, together with the use of the constitutive law. Instead, *RCP0* and *RCP1* denote the use of RCP as presented in Eq. (3.15), for *Patch 0* and *Patch 1*, respectively.

Figures 4, 5 and 6 report results obtained for *Test a*, *Test b* and *Test c* for all the aforementioned meshes, respectively. Aiming at providing a picture of the overall behaviour of the procedure, for each test, results obtained considering all structured meshes are plotted on the same graph differentiating them by means of the marker type. Analogously, all results related to unstructured meshes are represented together. Results obtained by means of *VEM*, *RCP0* and *RCP1* are plotted with continuous lines with black markers, dashed lines with red markers and dash-dot lines and blue markers, respectively.

It can be clearly seen that RCP always has a favourable effect, leading to more accurate results if compared to the use of the $\mathbf{\Pi}^m$ operator and, in some

cases, to a substantial increase in the convergence rate. Regarding *RCP0*, we notice that the improvement can be clearly appreciated when the Hex (S) mesh is considered while it tends to disappear for triangular elements. Furthermore, considering now results obtained using *RCP1*, it can be seen that the use of element patches has a significant beneficial effect, in agreement with what has been observed in the context of displacement-based finite elements [36, 37].

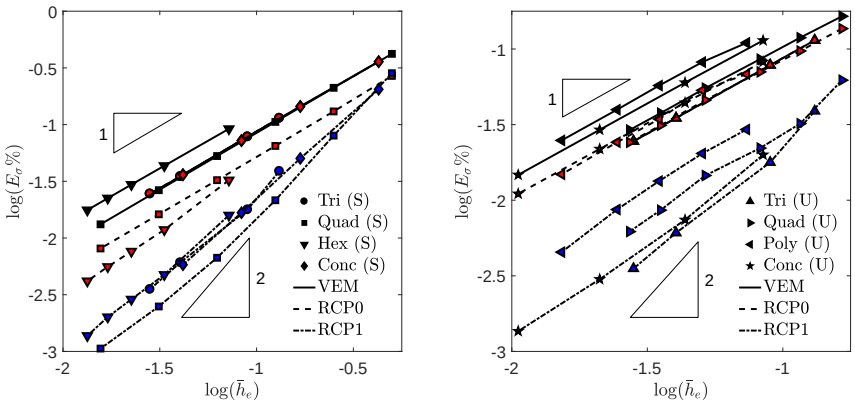

Figure 4: $\bar{h}_e-$convergence results for Test *a*: (a) structured and (b) unstructured meshes. Black, red and blue markers indicate *VEM*, *RCP0* and *RCP1*, respectively.

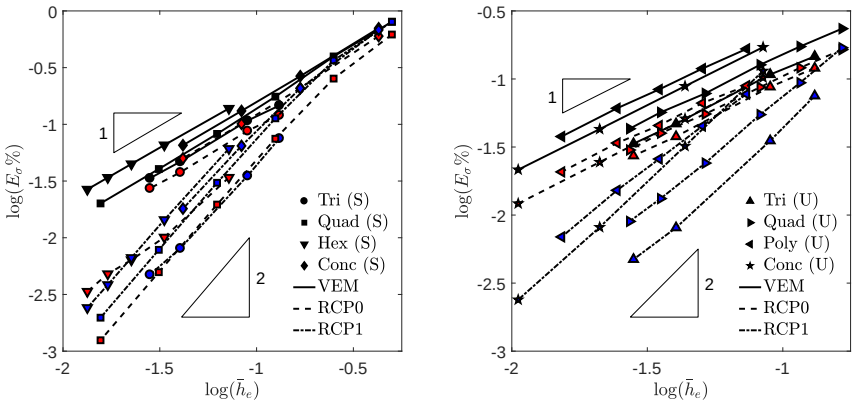

Figure 5: $\bar{h}_e-$convergence results for Test *b*: (a) structured and (b) unstructured meshes. Black, red and blue markers indicate *VEM*, *RCP0* and *RCP1*, respectively.

A comparison between the three techniques in terms of von Mises equivalent stress distributions obtained using Hex (S) and Poly (U) meshes is reported for

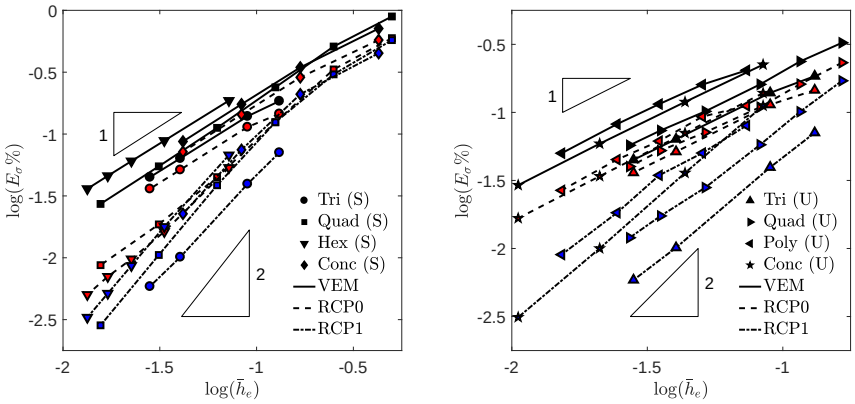

Figure 6: $\bar{h}_e-$convergence results for Test *c*: (a) structured and (b) unstructured meshes. Black, red and blue markers indicate *VEM*, *RCP0* and *RCP1*, respectively.

Test a and *Test b*. The exact solutions are shown in Fig. 7 while numerical results are reported in Figs. 8 and 9, respectively. The improved compliance with the analytical solution, even for relatively coarse meshes, can be clearly observed, confirming again the effectiveness of the proposed approach.

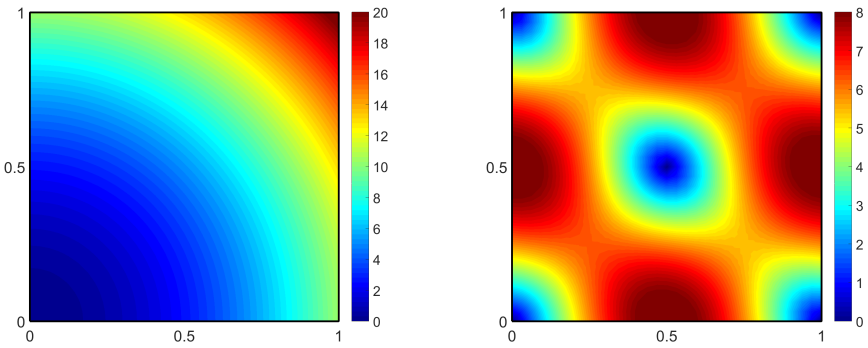

Figure 7: Exact von Mises equivalent stress distributions: (a) *Test a* and (b) *Test b*.

In order to further characterise the obtained results, sections of the stress field for *Test b* are reported in Fig. 10. In particular, a section extending from the lower left corner (denoted as P_A) to the upper right corner (denoted as P_B) of the plate is considered and the resulting segment parameterised by means of a coordinate s which is null at P_A and equal to unity at P_B. Such graphs are reported for all stress components for meshes Hex (S) and Poly (U) and considering both *RCP0* and *RCP1*. Although the method is developed in

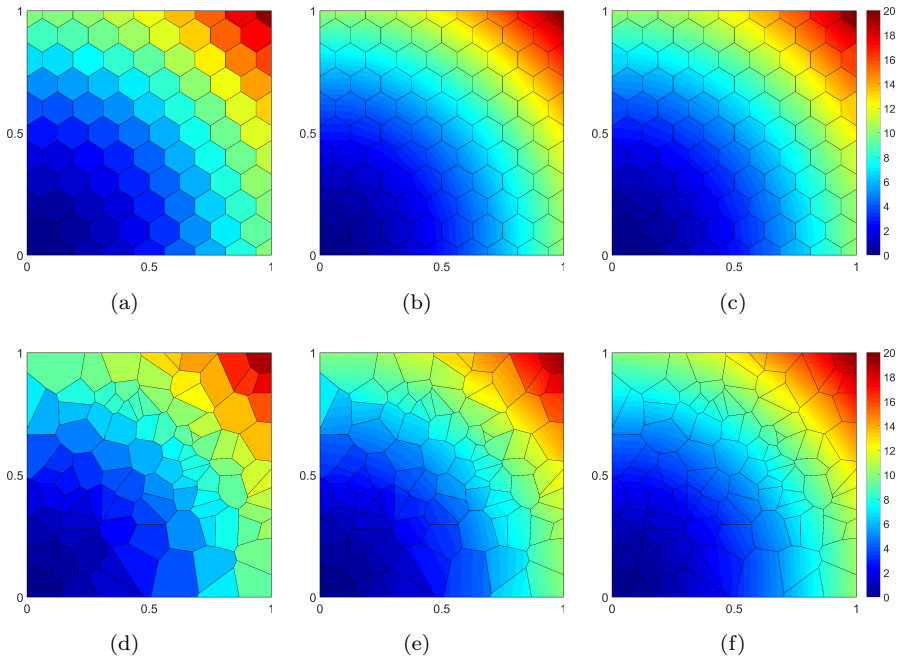

Figure 8: Von Mises equivalent stress distributions for *Test a*: (a) Hex (S) *VEM*, (b) Hex (S) *RCP0*, (c) Hex (S) *RCP1*, (d) Poly (U) *VEM*, (e) Poly (U) *RCP0* and (f) Poly (U) *RCP1*.

order to enforce equilibrium only in the interior of the elements, the jumps of the stress components across the edges are greatly reduced with respect to the VEM solution, so highlighting the good performance of the proposed procedure.

Finally, error maps are provided in order to characterise the spatial distribution of the obtained error energy. In particular, the following relative error energy measure is calculated for each element:

$$\bar{E}_{\sigma,E} = \log\left(\frac{\int_E (\boldsymbol{\sigma}^{ex} - \widetilde{\boldsymbol{\sigma}}_h)^T \boldsymbol{C}^{-1} (\boldsymbol{\sigma}^{ex} - \widetilde{\boldsymbol{\sigma}}_h)}{\int_E \boldsymbol{\sigma}^{exT} \boldsymbol{C}^{-1} \boldsymbol{\sigma}^{ex}}\right). \tag{4.2}$$

Figure 11 shows maps reporting the distribution of $\bar{E}_{\sigma,E}$ for *Test b* considering meshes Hex (S) and Poly (U). Once again, results confirm the soundness of the proposed approach showing an increase of the solution accuracy with respect to VEM when *RCP0* and *RCP1* are adopted.

4.1. Gaussian peak

In this section, a sensitivity study is performed in order to highlight how the results obtained by means of the proposed technique vary with respect to the peak sharpness of the problem solution. In particular, the analytical solution is selected to be a Gaussian function such that

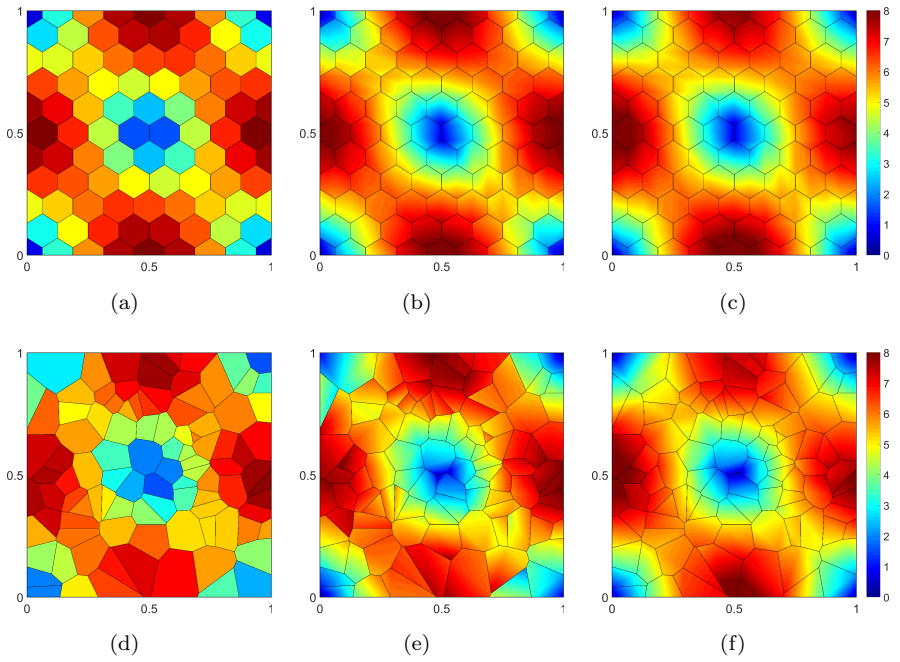

Figure 9: Von Mises equivalent stress distributions for *Test b*: (a) Hex (S) *VEM*, (b) Hex (S) *RCP0*, (c) Hex (S) *RCP1*, (d) Poly (U) *VEM*, (e) Poly (U) *RCP0* and (f) Poly (U) *RCP1*.

$$u_x = e^{-\frac{1}{2}\left(\frac{r}{L}\right)^2}, \; u_y = 0, \tag{4.3}$$

where r is the distance between the considered point and $[0.5, 0.5]$ while L, the standard deviation of the Gaussian distribution, can be varied in order to control the sharpness of the peak. In this case, the mesh is kept constant while body forces, boundary conditions and E_σ are calculated as already presented in Sec. 4. Notice that the information provided by such analyses is, to a great extent, similar to that presented in $\bar{h}_e-$convergence graphs but the attention is here focused on the peak sharpness of the solution rather than on the mesh refinement. In particular, Fig. 12 reports the E_σ with respect to L for Tri (S), Tri (U), Hex (S) and Poly (U) meshes. The L parameter is varied between 0.5 to 0.03.

It can be seen that, as expected, for meshes composed of triangular elements $RCP0$ is slightly different from the VEM solution due to the presence of the particular solution. When polygons characterised by numerous sides are present (Hex (S) and Poly (U) meshes), $RCP0$ can lead to more accurate results with respect to VEM due to a more suitable use of the information at the element boundaries. It appears that for all considered meshes and values of L, $RCP0$ always has at least the same accuracy of the VEM solution. Considering that such an approach does not need the creation of patches, this aspect strongly

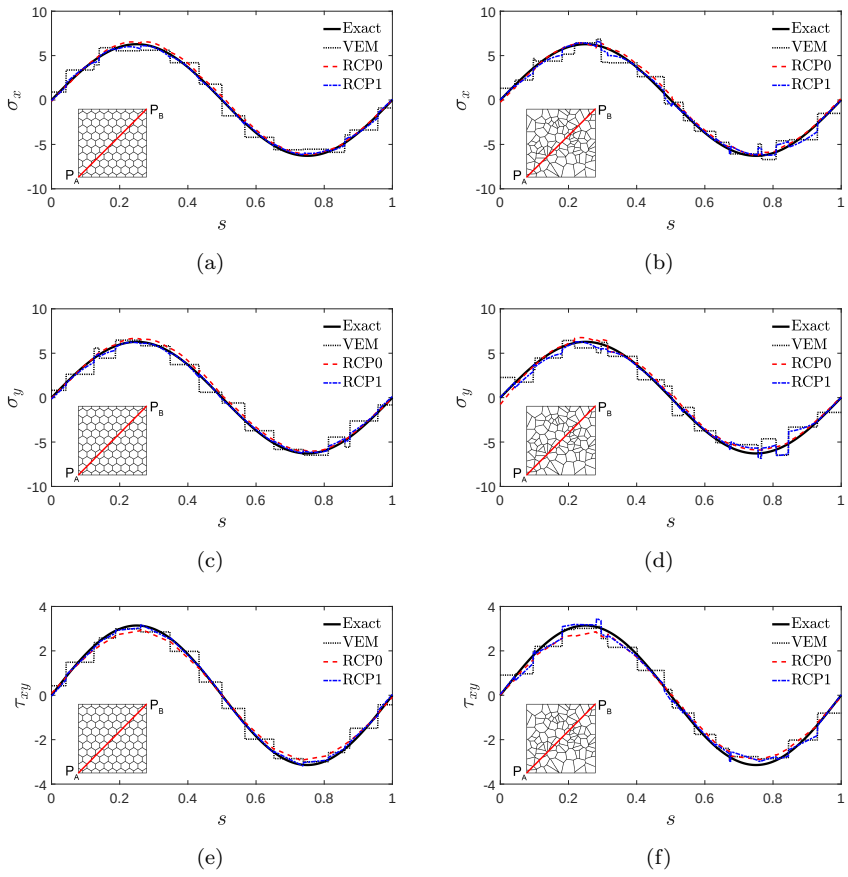

Figure 10: Sections of the stress field (the right column refers to Hex (S) while the left column refers to Poly (U)): (a) and (b) σ_x, (c) and (d) σ_y, (e) and (f) τ_{xy} .

advocates its use as a valid alternative to the standard stress evaluation procedure based on the projection operator. Furthermore, it can be observed that for very coarse meshes $RCP1$ tends to be less accurate than both VEM and $RCP0$. This is not unexpected as $RCP0$ and $RCP1$ share the same representation of the stress field but the first one recovers them on a much smaller domain with respect to the second one. Such effects are particularly unfavourable when the central element is eccentric with respect to the patch and, thus, are particularly strong for unstructured meshes. It should be nevertheless considered that $RCP1$ appears to be less accurate than VEM and $RCP0$ only for very coarse meshes, in which the energy error introduced by the numerical solution is comparable to the energy of the solution.

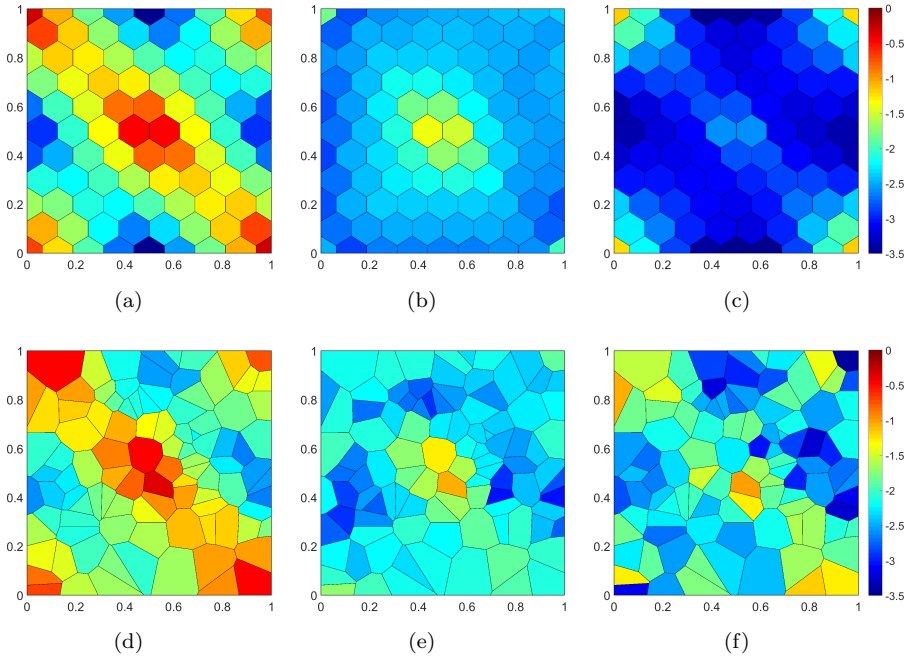

Figure 11: Maps of $\bar{E}_{\sigma,E}$: (a), (b) and (c) VEM, *RCP0* and *RCP1* for Hex (S) and (d), (e) and (f) VEM, *RCP0* and *RCP1* for Poly (U).

5. Conclusions

In the framework of the displacement-based virtual element methods, the standard approach to compute stresses is via the constitutive law, using the available approximated strains. When general polygons are considered, such a procedure does not fully exploit the adopted degrees of freedom, thus, leading to a quite poor stress field with respect to the available information.

In the present paper, the beneficial effects of using RCP in conjunction with VEM discretisation schemes have been presented. The RCP formulation allows to compute accurate pointwise equilibrated stress fields starting from approximated boundary displacements and from the knowledge of the applied loads. Such a formulation appears to be well-suited for the recovery of stresses in the framework of displacement-based virtual elements, in which such quantities are known only on the elements edges. In its simplest version, the RCP is applied elementwise, so representing an efficient alternative to the standard stress recovery. It has been also shown that further improvements might be obtained by considering patches of elements, in agreement with the results obtained in the context of finite elements schemes. We finally remark that RCP can be very easily integrated in existing codes without introducing significant computational costs.

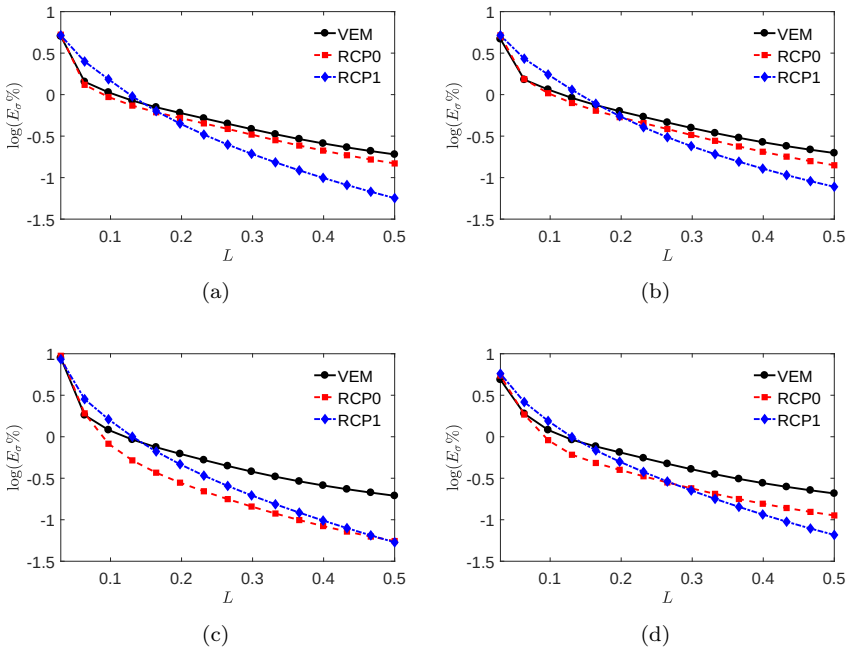

Figure 12: Graphs reporting the variation of E_σ with respect to L: (a) Tri (S), Tri (U), Hex (S), Poly (U).

Acknowledgements

E.A. gratefully acknowledges the partial financial support of University of Rome Tor Vergata Mission Sustainability Programme through project SPY-E81I18000540005.

Appendix A

The aim of this appendix is to provide a first mathematical justification of our stress recovery procedure. Accordingly, in this section we will use standard mathematical concepts and notations, such as Sobolev norms and semi-norms, see [46] and [47], for instance. Furthermore, given two nonnegative real quantities a and b, we will write $a \lesssim b$ if there exists a positive constant C, independent of the meshsize h, such that $a \leq C\, b$.

We point out that a detailed analysis, capable of explaining all the (possibly) superconvergence phenomena experienced in Section 4, is still missing. We however show that the stress recovery, starting from the approximate displacement solution, is convergent to the analytical stresses, at least with the same order as the computed discrete displacements.

With the symbols introduced in Section 3, the error of the recovered stress is:

$$\boldsymbol{\sigma} - \widetilde{\boldsymbol{\sigma}}_h = \boldsymbol{\sigma_0} - \widetilde{\boldsymbol{\sigma}}_{\mathbf{0},h} = (\boldsymbol{\sigma_0} - \widetilde{\boldsymbol{\sigma}}_{\mathbf{0}}) + (\widetilde{\boldsymbol{\sigma}}_{\mathbf{0}} - \widetilde{\boldsymbol{\sigma}}_{0,h}). \tag{A.1}$$

We have the following error estimate.

Proposition 5.1. *Suppose that the mesh satisfies the usual mesh assumptions (see [1], for example). Let us denote with* $(\boldsymbol{\sigma}, \mathbf{u})$ *the solution of the continuous problem* (3.1)*, and write* $\boldsymbol{\sigma}$ *using the splitting* (3.5)*. If* $\mathbf{u}_h$ *is the VEM solution of the primal problem* (2.2)*, and* $\widetilde{\boldsymbol{\sigma}}_h$ *is the recovered stress on an element (or patch)* E*, see* (3.8) *and* (3.9)*, then it holds*

$$||\boldsymbol{\sigma} - \widetilde{\boldsymbol{\sigma}}_h||_{L^2(E)} \lesssim |\mathbf{u} - \mathbf{u}_h|_{H^1(E)} + \inf\left\{||\boldsymbol{\sigma_0} - \boldsymbol{\tau}_{\mathbf{0},h}||_{L^2(E)} \ : \ \boldsymbol{\tau}_{\mathbf{0},h} \in \boldsymbol{\Sigma}_{\mathbf{0},h}(E)\right\}, \tag{A.2}$$

where $\boldsymbol{\sigma}_0$ *is defined in* (3.5)*.*

Proof. We use (A.1), and separately estimate the two error contributions.

Regarding $\boldsymbol{\sigma_0} - \widetilde{\boldsymbol{\sigma}}_0$, we subtract (3.7) from (3.6) to obtain

$$\int_E \boldsymbol{\tau}_{\mathbf{0}}^T \boldsymbol{C}^{-1}(\boldsymbol{\sigma_0} - \widetilde{\boldsymbol{\sigma}}_{\mathbf{0}}) = \int_{\partial E} (\mathbf{u} - \mathbf{u}_h)^T \boldsymbol{\mathcal{N}}_E \boldsymbol{\tau}_0 \qquad \forall \boldsymbol{\tau_0} \in \boldsymbol{\Sigma_0}(E). \tag{A.3}$$

Choosing $\boldsymbol{\tau_0} = \boldsymbol{\sigma_0} - \widetilde{\boldsymbol{\sigma}}_{\mathbf{0}}$ and applying the Gauss-Green theorem to the right-hand side, we get

$$\int_E (\boldsymbol{\sigma_0} - \widetilde{\boldsymbol{\sigma}}_{\mathbf{0}})^T \boldsymbol{C}^{-1}(\boldsymbol{\sigma_0} - \widetilde{\boldsymbol{\sigma}}_{\mathbf{0}}) = \int_E \boldsymbol{\varepsilon}(\mathbf{u} - \mathbf{u}_h)^T (\boldsymbol{\sigma_0} - \widetilde{\boldsymbol{\sigma}}_{\mathbf{0}}). \tag{A.4}$$

Using coercivity for the left-hand side and the Schwarz inequality for the right-hand side of (A.4), we deduce

$$||\boldsymbol{\sigma_0} - \widetilde{\boldsymbol{\sigma}}_{\mathbf{0}}||_{L^2(E)} \lesssim |\mathbf{u} - \mathbf{u}_h|_{H^1(E)}. \tag{A.5}$$

Regarding $\widetilde{\boldsymbol{\sigma}}_{\mathbf{0}} - \widetilde{\boldsymbol{\sigma}}_{\mathbf{0},h}$, we first remark that in $\boldsymbol{\Sigma_0}(E)$ the $H(\mathbf{D}^\star, E)$ norm equals the $L^2(E)$ norm. Then, we notice, see (3.7) and (3.8), that $\widetilde{\boldsymbol{\sigma}}_{\mathbf{0},h}$ is the Galerkin projection of $\widetilde{\boldsymbol{\sigma}}_{\mathbf{0}}$ for the stable problem (3.7). Therefore, the standard theory of Galerkin methods yields

$$||\widetilde{\boldsymbol{\sigma}}_{\mathbf{0}} - \widetilde{\boldsymbol{\sigma}}_{\mathbf{0},h}||_{L^2(E)} \lesssim \inf\left\{||\boldsymbol{\sigma_0} - \boldsymbol{\tau}_{\mathbf{0},h}||_{L^2(E)} \ : \ \boldsymbol{\tau}_{\mathbf{0},h} \in \boldsymbol{\Sigma}_{\mathbf{0},h}(E)\right\}. \tag{A.6}$$

From (A.1), using the triangle inequality and combining (A.5) and (A.6), we obtain the bound (A.2). □

We now notice that the standard VEM convergence theory gives:

$$|\mathbf{u} - \mathbf{u}_h|_{H^1(E)} = O(h_E), \tag{A.7}$$

h_E being the diameter of E.

To continue, the stress spaces we used for the recovery are, for $k \geq 1$:

$$\boldsymbol{\Sigma}_{\mathbf{0},h}(E) = \left\{ \boldsymbol{\tau}_{\mathbf{0},h} \in P_k(E)_s^{2\times 2} \ : \ \mathbf{D}^\star \boldsymbol{\tau}_{\mathbf{0},h} = \mathbf{0} \right\}, \tag{A.8}$$

where $P_k(E)_s^{2\times 2}$ denotes the space of symmetric tensors (here represented using Voigt notation) whose components are polynomials of degree at most k. For these spaces and for regular $\boldsymbol{\sigma}_\mathbf{0}$, the Scott-Dupont approximation theory leads to:

$$\inf \left\{ ||\boldsymbol{\sigma}_\mathbf{0} - \boldsymbol{\tau}_{\mathbf{0},h}||_{L^2(E)} \ : \ \boldsymbol{\tau}_{\mathbf{0},h} \in \boldsymbol{\Sigma}_{\mathbf{0},h}(E) \right\} = O(h_E^{k+1}). \tag{A.9}$$

In fact, since our problem is in 2D, if $\boldsymbol{\sigma}_\mathbf{0} \in \boldsymbol{\Sigma}_\mathbf{0}(E)$, then there exists the *Airy stress function* $\varphi \in H^2(E)$ such that $\boldsymbol{\sigma}_\mathbf{0} = Cof(H(\varphi))$. Here, $H(\varphi)$ is the Hessian of φ, and $Cof(A)$ denotes the cofactor matrix of the matrix A.

We notice that for every nonegative integer m, if $\boldsymbol{\sigma}_\mathbf{0} \in H^m(E)_s^{2\times 2}$, then $|\boldsymbol{\sigma}_\mathbf{0}|_{H^m(E)} = |\varphi|_{H^{m+2}(E)}$. Now, take $\varphi_I \in P_{k+2}(E)$ as the averaged Taylor expansion of φ (see [46], for instance), and set $\boldsymbol{\sigma}_{\mathbf{0},I} := Cof(H(\varphi_I))$. We have $\boldsymbol{\sigma}_{\mathbf{0},I} \in \boldsymbol{\Sigma}_{\mathbf{0},h}(E)$, together with the estimate:

$$||\boldsymbol{\sigma}_\mathbf{0} - \boldsymbol{\sigma}_{\mathbf{0},I}||_{L^2(E)} = |\varphi - \varphi_I|_{H^2(E)} \lesssim h_E^{k+1} |\varphi|_{H^{k+3}(E)} = h_E^{k+1} |\boldsymbol{\sigma}_\mathbf{0}|_{H^{k+1}(E)}, \tag{A.10}$$

which implies (A.9).

From Proposition 5.1, bounds (A.7) and (A.9), we get the estimate for the recovered stress:

$$||\boldsymbol{\sigma} - \boldsymbol{\sigma}_h^*||_{L^2(E)} \lesssim h_E. \tag{A.11}$$

Remark 1. *An alternative way to introduce the Airy stress function is to set:* $\boldsymbol{\sigma}_\mathbf{0} = \mathbf{Curl}\,\mathbf{curl}\,\varphi$.

Remark 2. *Estimate* (A.11) *shows that, in general, the recovered stress is first order convergent, even though the space* $\boldsymbol{\Sigma}_{\mathbf{0},h}(E)$ *would be capable of a higher order convergence rate (cf.* (A.9)*). Of course, this is caused by the low order approximation* $\mathbf{u}_h$ *we have at our disposal (cf.* (A.7)*). However, the numerical experiments of Section 4 highlight that our stress recovery is typically beneficial.*

Bibliography

[1] L. Beirão da Veiga, F. Brezzi, A. Cangiani, G. Manzini, L. D. Marini, and A. Russo, "Basic principles of Virtual Element Methods," *Math. Models Methods Appl. Sci.*, vol. 23, pp. 119–214, 2013.

[2] L. Beirão da Veiga, F. Brezzi, L. D. Marini, and A. Russo, "The Hitchhikers Guide to the Virtual Element Method," *Math. Models Methods Appl. Sci.*, vol. 24, no. 8, pp. 1541–1573, 2014.

[3] L. Beirão da Veiga, F. Brezzi, and L. D. Marini, "Virtual Elements for linear elasticity problems," *Siam. J. Numer. Anal.*, vol. 51, pp. 794–812, 2013.

[4] B. Ayuso, K. Lipnikov, and G. Manzini, "The nonconforming virtual element method." Preprint arXiv:1405.3741. Submitted for publication.

[5] P. Antonietti, L. Beirão da Veiga, D. Mora, and M. Verani, "A stream function formulation of the Stokes problem for the virtual element method," *Siam. J. Numer. Anal.*, vol. 52, pp. 386–404, 2014.

[6] F. Brezzi and L. Marini, "Virtual Element Method for plate bending problems," *Comput. Methods Appl. Mech. Engrg.*, vol. 253, pp. 455–462, 2012.

[7] E. Artioli, L. Beirão Da Veiga, C. Lovadina, and E. Sacco, "Arbitrary order 2D virtual elements for polygonal meshes: part I, elastic problem," *Comp. Mech.*, vol. 60, pp. 355–377, 2017.

[8] E. Artioli, L. Beirão Da Veiga, C. Lovadina, and E. Sacco, "Arbitrary order 2D virtual elements for polygonal meshes: part II, inelastic problem," *Comp. Mech.*, vol. 60, pp. 643–657, 2017.

[9] P. Wriggers, B. Reddy, W. Rust, and B. Hudobivnik, "Efficient virtual element formulations for compressible and incompressible finite deformations," *Computational Mechanics*, vol. 60, no. 2, pp. 253–268, 2017.

[10] H. Chi, L. Beirão da Veiga, and G. H. Paulino, "Some basic formulations of the virtual element method (VEM) for finite deformations," *Comput. Meth. Appl. Mech. Engrg.*, vol. 318, pp. 148–192, 2017.

[11] C. Talischi, G. Paulino, A. Pereira, and I. Menezes, "Polygonal finite elements for topology optimization: A unifying paradigm.," *Int. J. for Num. Meth. Engnr.*, vol. 82, pp. 671–698, 2010.

[12] P. Antonietti, M. Bruggi, S. Scacchi, and M. Verani, "On the virtual element method for topology optimization on polygonal meshes: a numerical study," *Computers and Mathematics with Applications*, vol. 74, pp. 1091–1109, 2017.

[13] M. Benedetto, S. Berrone, S. Pieraccini, and S. Scialò, "The Virtual Element Method for Discrete Fracture Network simulations.," *Comput. Meth. Appl. Mech. Engrg.*, vol. 280, pp. 135–156, 2014.

[14] I. Perugia, P. Pietra, and A. Russo, "The plane wave virtual element method for the Helmholtz problem." Submitted for publication.

[15] D. Mora, G. Rivera, and R. Rodríguez, "A virtual element method for the Steklov eigenvalue problem." CI2MA Pre-Publicación 2014-27, in press on Math. Mod. Meth. Appl. Math., 2015.

[16] A. Gain, C. Talischi, and G. Paulino, "On the Virtual Element Method for Three-Dimensional Elasticity Problems on Arbitrary Polyhedral Meshes," *Comp. Meth. Appl. Mech. Engrg.*, vol. 282, pp. 132–160, 2014.

[17] F. Brezzi, R. Falk, and L. Marini, "Basic principles of mixed Virtual Element Methods," *Math. Mod. Num. Anal.*, vol. 48, no. 4, pp. 1227–1240, 2014.

[18] E. Artioli, S. de Miranda, C. Lovadina, and L. Patruno, "A stress/displacement virtual element method for plane elasticity problems," *Comp. Meth. Appl. Mech. Engrg.*, vol. 325, pp. 155–174, 2017.

[19] E. Artioli, S. de Miranda, C. Lovadina, and L. Patruno, "A family of virtual element methods for plane elasticity problems based on the hellingerreissner principle," *Comp. Meth. Appl. Mech. Engrg.*, vol. 340, pp. 978–999, 2018.

[20] M. Ainsworth and J. Oden, *A posteriori error estimation in finite element analysis*. Hoboken: John Wiley & Sons, 2011.

[21] O. Zienkiewicz and J. Zhu, "The superconvergent patch recovery and a posteriori error estimates. Part I: the recovery technique," *Int. J. Numer. Methods. Eng.*, vol. 33, pp. 1331–1364, 1992.

[22] O. Zienkiewicz and J. Zhu, "The superconvergent patch recovery and a posteriori error estimates. Part II: error estimates and adaptivity," *Int. J. Numer. Methods. Eng.*, vol. 33, pp. 1365–1382, 1992.

[23] T. Blacker and T. Belytschko, "Superconvergent patch recovery with equilibrium and conjoint interpolant enhancements," *Int. J. Numer. Methods. Eng.*, vol. 37, pp. 517–536, 1994.

[24] N. Wiberg and F. Abdulwahab, "Error estimation and adaptive procedures based on superconvergent patch recovery (SPR) techniques," *Arch. Comput. Methods Eng.*, vol. 4, pp. 203–242, 1997.

[25] T. Lee, H. Park, and S. Lee, "A superconvergent stress recovery technique with equilibrium constraint," *Int. J. Numer. Methods Eng.*, vol. 40, pp. 1139–1160, 1997.

[26] H. Park and S. Shin, "Element stress recovery technique with equilibrium constraints for superconvergence boundary stress extraction," *AIAA J*, vol. 37, pp. 623–628, 1999.

[27] T. Kvamsdal and K. Okstad, "Error estimation based on superconvergent patch recovery using statically admissible stress fields," *Int. J. Numer. Methods Eng.*, vol. 42, pp. 443–472, 1998.

[28] K. Okstad, T. Kvamsdal, and K. Mathisen, "Superconvergent patch recovery for plate problems using statically admissible stress resultant fields," *Int. J. Numer. Methods Eng.*, vol. 44, pp. 697–727, 1999.

[29] B. Boroomand and O. Zienkiewicz, "Recovery by equilibrium in patches (REP)," *Int. J. Numer. Methods Eng.*, vol. 40, pp. 137–164, 1997.

[30] B. Boroomand and O. Zienkiewicz, "An improved REP recovery and the effectivity robustness test," *Int. J. Numer. Methods Eng.*, vol. 40, pp. 3247–3277, 1997.

[31] B. Boroomand, O. Zienkiewicz, and J. Zhu, "Recovery procedures in error estimation and adaptivity. Part I: adaptivity in linear problems," *Comput. Methods Appl. Mech. Eng.*, vol. 176, pp. 111–125, 1999.

[32] P. Ladevéze and E. Maunder, "A general method for recovering equilibrating element tractions," *Comput. Methods Appl. Mech. Eng.*, vol. 137, pp. 111–151, 1996.

[33] J. Moitinho de Almeida and E. Maunder, "Recovery of equilibrium on star patches using a partition of unity technique," *International Journal for Numerical Methods in Engineering*, vol. 79, pp. 1493–1516, 2009.

[34] N. Perés, P. Díez, and A. Huerta, "Exact bounds for linear outputs of the advection-diffusion-reaction equation using flux-free error estimates," *SIAM Journal on Scientific Computing*, vol. 31, pp. 3064–3089, 2009.

[35] N. Perés and P. Díez, "A new equilibrated residual method improving accuracy and efficiency of flux-free error estimates," *Computer Methods in Applied Mechanics and Engineering*, vol. 313, pp. 785–816, 2017.

[36] F. Ubertini, "Patch recovery based on complementary energy," *Int. J. for Num. Meth. Engnr.*, vol. 59, pp. 1501–1538, 2004.

[37] A. Benedetti, S. de Miranda, and F. Ubertini, "A posteriori error estimation based on the superconvergent recovery by compatibility in patches," *Int. J. for Num. Meth. Engnr.*, vol. 67, pp. 108–131, 2006.

[38] G. Castellazzi, S. de Miranda, and F. Ubertini, "Adaptivity based on the recovery by compatibility in patches," *Finite Elements in Analysis and Design*, vol. 46, pp. 379–390, 2010.

[39] S. de Miranda, L. Patruno, and F. Ubertini, "Transverse stress profiles reconstruction for finite element analysis of laminated plates," *Comp. Stru.*, vol. 94, pp. 2706–2715, 2012.

[40] E. Artioli, S. de Miranda, C. Lovadina, and L. Patruno, "A family of virtual element methods for plane elasticity problems based on the hellinger-reissner principle," *Comp. Meth. Appl. Mech. Engrg., submitted*.

[41] D. Boffi, F. Brezzi, and M. Fortin, *Mixed finite element methods and applications*, vol. 44 of *Springer Series in Computational Mathematics*. Springer, Heidelberg, 2013.

[42] F. de Veubeke, *Matrix Methods of Structural Analysis*. Pergamon Press, 1964.

[43] T. Pian and P. Tong, "Basis of finite element methods for solid continua," *Int. J. Numer. Methods Eng.*, vol. 1, pp. 3–28, 1969.

[44] F. Daghia, s. de Miranda, and F. Ubertini, "Patch based recovery in finite element elastoplastic analysis," *Computational Mechanics*, vol. 52, pp. 827–836, 2013.

[45] L. B. da Veiga, C. Lovadina, and D. Mora, "A Virtual Element Method for elastic and inelastic problems on polytope meshes," *Computer Methods in Applied Mechanics and Engineering*, vol. 295, pp. 327 – 346, 2015.

[46] S. Brenner and L. Scott, *The Mathematical Theory of Finite Element Methods*. Berlin/Heidelberg: Springer-Verlag, 1994.

[47] P. G. Ciarlet, *The Finite Element Method for Elliptic Problems*. Amsterdam: North-Holland, 1978.